J Mater Sci: Mater Med (2014) 25:669–680
DOI 10.1007/s10856-013-5111-2

Novel mineralized heparin–gelatin nanoparticles for potential application in tissue engineering of bone

Yuan Yang · Haihao Tang · Alexander Köwitsch · Karsten Mäder · Gerd Hause · Joachim Ulrich · Thomas Groth

Received: 6 May 2013 / Accepted: 29 November 2013 / Published online: 6 December 2013
© Springer Science+Business Media New York 2013

Abstract Nanoparticles (NPs) were prepared from succinylated gelatin (s-GL) cross-linked with aldehyde heparin (a-HEP) and used subsequently as a nano-template for the mineralization of hydroxyapatite (HAP). Gelatin was functionalized with succinyl groups that made it soluble at room temperature. Heparin was oxidized to generate aldehyde groups and then used as a cross-linker that can react with s-GL to form NPs via Schiff's base linkage. The polymer concentrations, feed molar ratios and pH conditions were varied to fabricate NPs suspension. NPs were obtained with a spheroid shape of an average size of 196 nm at pH 2.5 and 202 nm at pH 7.4. These NPs had a positive zeta potential of 7.3 ± 3.0 mV and a narrow distribution with PDI 0.123 at pH 2.5, while they had a negative zeta potential of −2.6 ± 0.3 mV and formed aggregates (PDI 0.257) at pH 7.4. The NPs prepared at pH 2.5 with a mean particle size of 196 nm were further used for mineralization studies. The mineralization process was mediated by solution without calcination at 37 °C. The HAP formed on NPs was analyzed by Fourier transform infrared spectroscopy and X-ray diffraction. HAP coated s-GL/a-HEP NPs developed in this study may be used in future as osteoinductive fillers enhancing the mechanical properties of injectable hydrogel or use as potential multifunctional device for nanotherapeutic approaches.

Yuan Yang and Haihao Tang have contributed equally to this study.

Electronic supplementary material The online version of this article (doi:10.1007/s10856-013-5111-2) contains supplementary material, which is available to authorized users.

Y. Yang · H. Tang · A. Köwitsch · T. Groth (✉)
Biomedical Materials Group, Department of Pharmaceutical Technology and Biopharmacy, Institute of Pharmacy, Martin Luther University Halle-Wittenberg, Heinrich-Damerow-Str. 4, 06120 Halle (Saale), Germany
e-mail: thomas.groth@pharmazie.uni-halle.de

K. Mäder
Pharmaceutical Technology Group, Department of Pharmaceutical Technology and Biopharmacy, Institute of Pharmacy, Martin Luther University Halle-Wittenberg, Wolfgang-Langenbeck-Str. 4, 06120 Halle (Saale), Germany

G. Hause
Microscopy Unit, Biocenter, Martin Luther University Halle-Wittenberg, Weinberg Weg 22, 06120 Halle (Saale), Germany

J. Ulrich
Thermal Process Engineering, Center for Engineering Science, Martin Luther University Halle-Wittenberg, Hoher Weg 7, 06120 Halle (Saale), Germany

1 Introduction

Natural bone is composed of 30 % w/v organic collagen fibrils and 70 % inorganic calcium phosphate crystals, hierarchically organized at nanoscale, which has been used as model for different attempts to mimic the bone structure on a nanoscale level [1–3]. Composite polymeric matrices were developed that combine the inorganic component of bone namely calcium phosphates (CaP) like hydroxyapatite (HAP) with polymeric materials such as chitosan obtain injectable nanocomposite systems that possess compositional and partly structural analogies to natural bone [4, 5]. Classical HAP-polymer composites were fabricated at macroscale due to the requirement of critical size defects. Recently, HAP or CaP/polymer nanocomposites were developed, which enable these hybrid materials to extend their applications in the field of controlled drug delivery [6], minimal-invasive surgery and imaging [6, 7], which paves the way to new nanotherapeutic approaches. Particular HAP coated or mixed microspheres [8] or

nanoparticles (NPs) [2, 9] have attracted great interest, because of the feasibility to be used as regenerative filler or as a template for nucleation of new bone growth. However, only a few studies on engineering of CaP or HAP/gelatin NPs have been reported so far [2, 9]. The materials in these studies were fabricated using glutaraldehyde as a cross-linker via microemulsion technique, which resulted in NPs with a mean size of around 300 nm.

Gelatin is a protein produced by partial hydrolysis of collagen, which has been widely used as material in the pharmaceutics or food industry. Since collagen is a main matrix for bio-mineralization of HAP in nature, gelatin also evoked interest in the field of bone repair and regeneration. It can form transparent elastic thermo-reversible gels upon cooling around 35 °C due to the formation of collagen-like triple-helix [10], which can build up the shell of micro or nanocapsules for the controlled release of DNA [11] or growth factors [12, 13]. However, the gelatin shell layer is not stable enough in controlled release systems, because the body temperature is above the critical gel point or due to a decrease of extracellular pH value in tumor tissues [14]. Therefore, cross-linkers, like formaldehyde, glutaraldehyde or epoxy compounds are usually used to stabilize the particles or capsules during the formation procedure. However, the cytotoxity of these compounds has raised serious concerns about their safety and prompted research into the development of natural cross-linking reagents, like genipin [15]. Boanini et al. [8] also developed gelatin microspheres stabilized by dialdehyde alginate using an inverse microemulsion, but alginate lacks multiple bio-specific binding sites for growth factors or extracellular matrix proteins.

Heparin is a highly sulfated negatively charged glycosaminoglycan (GAG), which can non-covalently bind to various functional proteins, such as growth factors, extracellular matrix components and adhesion molecules, triggering multiple downstream signaling pathways [16] controlling cellular growth, differentiation and functions [17]. Thereby, the sulfation of heparin has a great influence on the interactions with proteins and cells. It has been reported that 2–O-sulfation from iduronic acid residues and 6–O-sulfation of glucosamine residues within heparin is essential in FGF-2 signal transduction [18, 19], while *N*-sulfate and 3–O-sulphation is required for its anticoagulant activity [19]. Heparin is also well known to interact with BMP-2, by which up-regulates the BMP-2-induced osteogenic activity through the contributions of BMP-2 antagonists and inhibitory Smads [20]. Jeon et al. [21] have synthesized heparin-conjugated nanospheres suspended in a fibrin gel, which can enhance BMP-2-induced ALP activity of osteoblasts and further stimulate bone formation and calcium deposition in vivo. Liu et al. [22] showed that polyelectrolyte nanoscale multilayers composed of HEP and chitosan promoted differentiation of hMSC towards osteoblasts, which further might promote bio-mineralization.

The vicinyl hydroxyl groups of GAGs can be oxidized and thereby generate active aldehyde groups, which can react with amino groups of other biopolymers, such as chitosan, gelatin or collagen. It has been also shown that oxidized GAGs like aldehyde hyaluronic acid is not cytotoxic up to 0.1 g/mL [23]. We also reported that immobilized aldehyde hyaluronic acid (HA) had similar bioactivity like native HA regarding the binding to its natural partner aggrecan [24]. In this work we generate aldehyde groups in heparin by oxidation, which shall act as biocompatible macromolecular cross-linker, to cross-link succinylated gelatin (s-GL) at room temperature and to form protein/GAG NPs by adjusting pH value and other parameter during the formation of particles. In addition, subsequent mineralization of NPs was performed using them as nucleation sites for complexing Ca^{2+} to acidic groups of s-GL and aldehyde heparin (a-HEP).

2 Materials and methods

2.1 Materials

Gelatin (Type A, bloom 80) was obtained from Fluka (Schnelldorf, Germany), heparin from Serva (Heidelberg, Germany) and succinic anhydride from Alfa Aesar (Karlsruhe, Germany). Sodium periodate, L-lysine, 2,4,6-trinitrobenzene sulfonic acid (TNBS) and Schiff's fuchsin-sulfite reagent were purchased from Sigma-Aldrich (Schnelldorf, Germany). The dialysis bag (Spectra/Por membrane, Mw cutoff = 3,500), acetone, glutaraldehyde, hydrochloric acid, sodium hydroxide and ammonia were obtained from Carl Roth GmbH (Karlsruhe, Germany). Sodium dodecyl sulfate (SDS) and Pluronic F68 were purchased from AppliChem (Gatersleben, Germany). Diammonium phosphate and calcium nitrate were bought from Merck (Darmstadt, Germany).

2.2 Preparation and characterization of protein and polysaccharide derivatives

2.2.1 Synthesis of s-GL and a-HEP

Succinylated gelatin was prepared (see Fig. 1a) as previously described [25]. Briefly, 50 mL of 5 % w/v gelatin solution was dissolved at 40 °C. The solution was adjusted to pH 9.0 by dropwise addition of 1 M NaOH solution. 0.625 g of succinic anhydride in 5 mL acetone was added to the gelatin solution, to obtain a ratio of 0.25 mg of succinic anhydride per milligram of gelatin. After addition

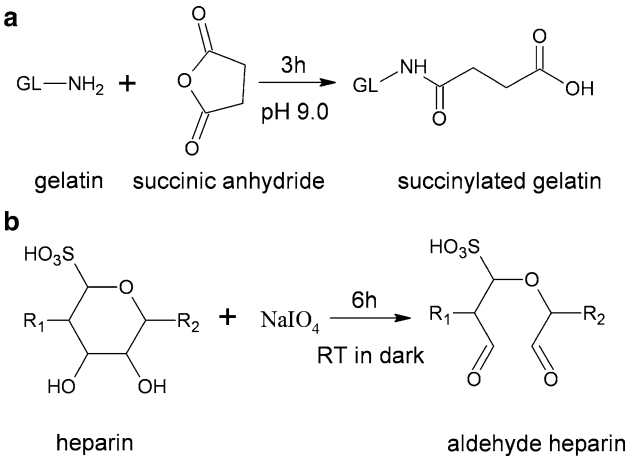

Fig. 1 Reaction scheme for the synthesis of components for the formation of NPs **a** succinylation of gelatin (s-GL) and **b** oxidation of heparin (a-HEP) (R_1, R_2 are vicinal saccharide units)

of succinic anhydride, the solution was stirred for 3 h at pH 9.0. s-GL was purified by dialysis against distilled water for 2 d and freeze-dried (ALPHA 1–2 LD plus, Christ, Osterode am Harz, Germany) overnight.

The method used for synthesis of a-HEP (Fig. 1b) was slightly modified compared to previous reports [24, 26]. A 0.4 % w/v heparin solution in distilled water was reacted with stoichiometric amounts of $NaIO_4$ at room temperature in the dark under constant stirring for 6 h. The amount of periodate was varied to obtain different degrees of oxidation. The solution was purified by dialysis against distilled water for 2 days. The final dry product was obtained by freeze-drying and stored at 4 °C.

2.2.2 *Characterization of s-GL and a-HEP*

2.2.2.1 Chemical structures and functional groups analysis The chemical structures of native molecules and their derivatives were analyzed by Fourier Transform Infrared (FTIR) spectroscopy (IFS 28, Bruker, Ettlingen, Germany). The functional groups, either amino groups or aldehyde groups, were determined by ultraviolet–visible (UV–Vis) spectroscopy using a modified procedure of TNBS assay [27] for amino groups and Schiff's reagent for aldehyde groups [24], respectively.

2.2.2.2 Molecular weight and polydispersity analysis The molecular weight and polydispersity of native molecules and their derivatives were measured by asymmetrical flow field-flow fractionation (FFF) equipped with a Dawn EOS detector (Wyatt Technology Corporation, Santa Barbara, CA, USA) and a refractive index (RI)-detector (Shodex RI-101, Showa Denko Europe GmbH, Munich, Germany). All samples with concentrations of 1 mg/mL were prepared in 50 mM NaCl with 0.02 % NaN_3 (w/v) to prevent bacterial growth. Molecular weights were calculated using Astra software (Wyatt Technology Corporation).

2.3 Preparation and characterization of s-GL/a-HEP NPs and HAP coated NPs

2.3.1 *Preparation of s-GL/a-HEP NPs*

To synthesize s-GL/a-HEP NPs, 10 mL of Pluronics F68 (0.1 and 1 % w/v) was prepared with MilliQ water and subsequently added to different amounts of s-GL (see result section) to obtain a final s-GLconcentration of 0.5 and 5 % w/v respectively according to previous work [28] After stirring for 0.5 h, the solution was filtrated with cellulose membrane (0.45 μm) and the pH was adjusted to 2.5 using 1 N HCl and 5.0, 7.4 and 10.0 with 1 N NaOH (for the parallel groups, respectively). 20 mL of acetone was dropped into the solution using a syringe pump (KDS 200, kdScientific, USA) at 1 mL/min dropping speed under stirring at 600 rpm for 20 min. The diameter of the needle was 0.5 mm. After stirring for 10 min, different amounts of a-HEP solution of concentration of 5 % w/v in DI water[n(–CHO)/n(–NH_2) = 10/2.3, 5/2.3, 1/2.3) were added to s-GL solution to form cross-linked NPs and stirred for 12 h. [9, 29] After that, acetone was evaporated over night at room temperature under a chemical hood and then the solution was centrifuged (Avanti J-26 XP, Beckman, USA) at 10,000 rpm for 5 min [30]. The sediment (particles bigger than 1 μm and some aggregates) was discarded and the solution was diluted to 25 mL with DI water. The nanoparticle solutions were stored at room temperature. The yield of NPs was calculated from the freeze-dried products and ended up with approximately 80 % w/w.

2.3.2 *Biomimetic HAP mineralization on s-GL/a-HEP NPs*

HAP mineralization on s-GL/a-HEP NPs was carried out as described previously [2, 8, 31]. 10 mL of s-GL/a-HEP nanoparticle solution was prepared. The pH was adjusted to 10.0 using $NH_3{\cdot}H_2O$. 0.0354 g $Ca(NO_3)_2{\cdot}4H_2O$ was added to the solution with a given ratio of 5 mmol Ca^{2+}/g s-GL/a-HEP NPs. The solution was stirred for 2 h at 37 °C. After that, to obtain Ca/P = 1.67, 5 mL of $(NH_4)_2HPO_4$ solution which contains 0.0238 g $(NH_4)_2HPO_4$ was dropped using syringe pump (KDS 200, kdScientific, USA) at 0.1 mL/min dropping speed under magnetic stirring at 600 rpm. The diameter of the needle was 0.5 mm. The pH of solution was then adjusted to 10.0 again using $NH_3{\cdot}H_2O$. At different reaction time points, 0.5, 1, 4 and 24 h, respectively, 3 mL of solution was removed and freeze-dried to obtain dry products for further analysis.

2.3.3 Characterization of s-GL/a-HEP NPs

2.3.3.1 Fourier transform infrared spectroscopy A FTIR spectrometer (IFS 28, Bruker, Ettlingen, Germany) was used to analyze the chemical composition of NPs and HAP coated NPs. The freeze-dried NPs were mixed with KBr to form pellets and examined on a spectrometer with a resolution of 2.00 cm^{-1} and recorded in the range of 4,000–400 cm^{-1}.

2.3.3.2 Dynamic light scattering (DLS) measurements Sizes and size distribution of NPs prepared at different pH conditions were characterized by DLS on a Zetasizer Nano NS (Malvern Instruments, Worcestershire, England), equipped with a detector to measure the intensity of the scattered light at 173° to the incident beam. The DLS measurements give a value called Z-average size (or cumulant mean), which is an intensity mean and the polydispersity index (PDI). The particle solution was measured in concentrations between 1 and 5 mg/mL at room temperature (25 °C).

2.3.3.3 Zeta-potential measurement Zeta-potentials of NPs at pH 2.5 and pH 7.4 were measured by Zetasizer Nano NS (Malvern Instruments, Worcestershire, England). All the samples of concentration of 1–5 mg/mL were dissolved in 10 mM NaCl in order to increase the conductivity which is between 1 and 5 mS/cm. The data were analyzed using the Malvern zetasizer v 6.30 software.

2.3.3.4 Transmission electron microscopy (TEM) Negatively stained samples were prepared by spreading 3 μL of the NPs dispersion onto a cupper grid (200 mesh) coated with a formvarfilm. After 1 min, excess liquid was blotted off with filter paper. The grid was then placed on a droplet of 1 % (w/v) aqueous uranyl acetate solution and drained off after 1 min. The dried specimens were examined with a Zeiss EM 900 transmission electron microscope at an acceleration voltage of 80 kV. Electron micrographs were taken with a slow scan camera (Variospeed SSCCD camera SM-1k-120, TRS, Moorenweis, Germany). The data were analyzed using Image J software.

2.3.3.5 Degree of cross-linking of NPs The free amino group content of NPs was quantified using a slightly modified TNBS test according to a previous report [32]. The NPs were dispersed in 4 % w/v $NaHCO_3$ to obtain 4 mg/mL sample solution. 1 mL of this solution was added with 1 mL of 0.1 % (w/w) TNBS in 4 % w/v $NaHCO_3$ (~pH 9.0). The mixture was stirred for 4 h at 40 °C. Then 1 mL of 10 % SDS and 0.5 mL of 1 M HCl were added to the mixture. 1 mL of 4 % w/v $NaHCO_3$ was used as a blank instead of a sample solution. The absorbance of the solution was measured at 365 nm using UV–Vis spectroscopy and compared to a plotted calibration curve using L-lysine as standard substance. The degree of cross-linking (D_c) of NPs was calculated from Eq. (1) by measuring the remaining free amino groups content within s-GL/a-HEP NPs.

$$D_c = \frac{(\text{Amino groups before crosslinking}) - (\text{Amino groups after crosslinking})}{(\text{Amino groups before crosslinking})} \times 100 \quad (1)$$

2.3.3.6 X-ray diffractometer (XRD) The mineralized NPs were investigated by XRD with a D4 ENDEAVOR XRD (BRUKER axs). A copper anode was used and the wavelength was 15.4 nm. 35 kV and 30 mA were used with the diffractometer. The XRD data were collected at room temperature (25 °C) over the 2-θ range of 10°–60° at step sizes of 0.02° and a count rate of 0.5 s/step. The software EVA v 8.0 was used for data analysis.

3 Results and discussion

3.1 Synthesis of s-GL and a-HEP

Gelatin type A used in this study can be dissolved in water at around 40 °C. At room temperature, it undergoes gelation due to the aggregation of collagen-like triple-helix. Gelatin was succinylated by using succinic anhydride (see Fig. 1a) to increase its water solubility [25] at room temperature, which is due to increased quantity of carboxylic groups and partially destruction of hydrogen bonds in the helix structure [25]. Vicinal hydroxyl groups of β-D-glucuronic acid or α-L-iduronic acid in heparin can be oxidized to dialdehydes in the presence of sodium periodate [24], which introduces these reactive groups to the sugar backbone (Fig. 1b) that can further react with amino group containing biopolymers.

The FTIR spectra of gelatin (GL), s-GL, heparin (HEP) and a-HEP are shown in Fig. 2. The spectrum of native GL (see Fig. 2c) has typical peaks at 1,634 and 1,533 cm^{-1}, which were associated to amide I [ν(C=O)] and amide II [δ(NH) and ν(N–C=O)] bands, respectively [25]. Compared with gelatin, a new weak absorption band (Fig. 2d)

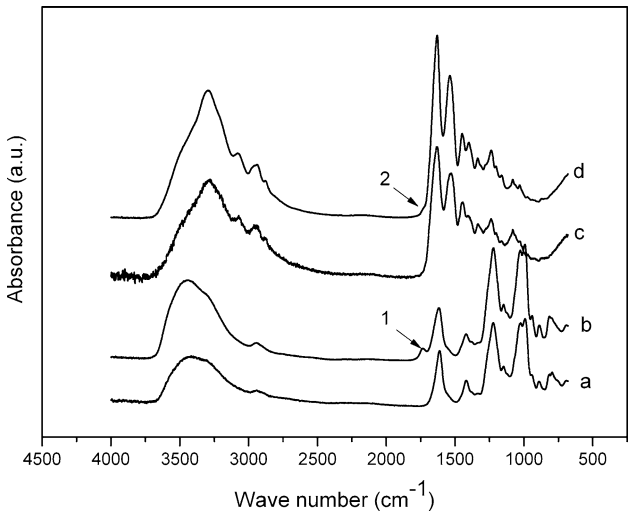

Fig. 2 FTIR spectra of *a* heparin, *b* a-HEP, *c* gelatin and *d* s-GL, and their new adsorption bands after chemical modification: (*1*)–C=O stretching vibration of aldehyde after oxidation, (*2*)–C=O stretching vibration of carboxyl groups after succinylation

Table 1 Active group contents (related to repeating disaccharide units) and weight average molecular mass (Mw), number average molar mass (Mn), and polydispersity index (PDI) of native molecules and their derivatives

Samples	Active groups contents		Molecular weight[b] (kDa)		
	$-NH_2$ group content[a] ($\times 10^{-4}$ mol/g)	–CHO group content[b] ($\times 10^{-4}$ mol/g)	Ww (kDa)	Wn (kDa)	PDI[c] (Mw/Mn)
GL	2.8	–	~190	~127	1.5
s-GL	1.1	–	~177	~42	4.2
HEP	–	–	~15.2	~14.0	1.1
a-HEP	–	10.0	~14.2	~12.4	1.1

[a] Amino groups content was determined via using TNBS assay by UV–Vis spectroscopy at 365 nm. L-lysine was used as the standard substance

[b] Molecular weights and PDI of native molecule and their derivatives were determined by field–flow fractionation with mobile phase of NaCl 50 mM

[c] Aldehyde content was determined via using Schiff's reagent by ultraviolet–visible (UV–Vis) spectroscopy at 550 nm. Glutardialdehyde was used as standard substance

appeared at 1,735 cm^{-1}, which was attributed to carboxyl groups (–COOH). This is in accordance with the work of Xiao et al. [25] and similar to the analogous synthesis of succinylated chitosan [33, 34], indicating that gelatin has been successfully modified. The spectrum of native heparin (see Fig. 2a) has typical peaks of saccharide alkyls at 2,920 and 1,415 cm^{-1}, alkoxyls at 1,040 cm^{-1} and sulfates at 1,231 and 1,029 cm^{-1} [35]. When heparin was oxidized, a new weak infrared band associated with the C=O stretch vibration of aldehyde groups appeared at 1,738 cm^{-1} (see Fig. 2b), which is in the agreement with the spectrum of oxidation of other GAGs, such as oxidized HA [24] or oxidized chondroitin sulfate (CS) [36].

Primary amino groups of GL and s-GL can react with TNBS (2,4,6-trinitrobenzenesulfonic acid) at alkaline pH conditions to form a color trinitrophenyl complex, which can be analyzed by UV–Vis spectroscopy at the wavelength of 365 nm [37, 38]. The amino group contents of gelatin and s-GL are shown in Table 1. The introduction of additional carboxyl groups to gelatin after succinylation can disturb hydrogen bonding, which in turn makes the protein more hydrophilic and anionic. It was found here that about 40 % of amino groups, 1.1×10^{-4} mol/g, of gelatin are still available after succinylation to react with aldehyde groups aHEP for NPs formation.

The controlled periodate oxidation of heparin should lead to the opening of the vicinal hydroxyls of glucuronic acid or iduronic acid rings, resulting in the formation of two aldehydes per ring. The amount of aldehydes of a-HEP was determined using Schiff's reagent and detected by UV–Vis spectroscopy at a wavelength of 550 nm within 40 min. The aldehyde groups of a-HEP had a molar concentration of 10.0×10^{-4} mol/g, which means approximately a 30 % degree of oxidation.

The molecular weights and PDI of the products were determined by FFF in 50 mM NaCl solution as the mobile phase. After succinylation, there were no significant molecular weight differences between gelatin and s-GL. After heparin oxidation, no significant degrease of a-HEP molecule weight was found. Since radicals may also break to glycosidic bonds and hence cause a decrease of molecular weight of GAG [24], it suggests that the oxidation procedure had little effect on the glycosidic bonds of heparin.

3.2 Synthesis of s-GL/a-HEP cross-linked NPs

Cross-linked s-GL/a-HEP NPs were prepared at different pH values probably by different reaction mechanisms according to Farris et al. [39]. At neutral or slightly alkaline conditions, the formation of NPs should be dominated by the formation of Schiff base linkage between non-protonated ε-NH_2 groups of s-GL and aldehyde groups of a-HEP (see Fig. 3a). By contrast, at acid condition (lower than 4.5), the reaction should take place between hydroxyl groups and aldehyde groups (see Fig. 3b). The acidic medium turns the α-carbon of the aldehyde into a highly reactive carbocation, and the –OH groups of hydroxyproline and hydroxylysine in gelatin (approximately 9.8 and 0.75 %, respectively, in type A gelatin) can attack it to form a hemiacetal. In addition, the electrostatic interactions between the positively charged $-NH_3^+$ and negatively charged $-COO^-$ or $-SO_3^{2-}$ groups may also contribute to

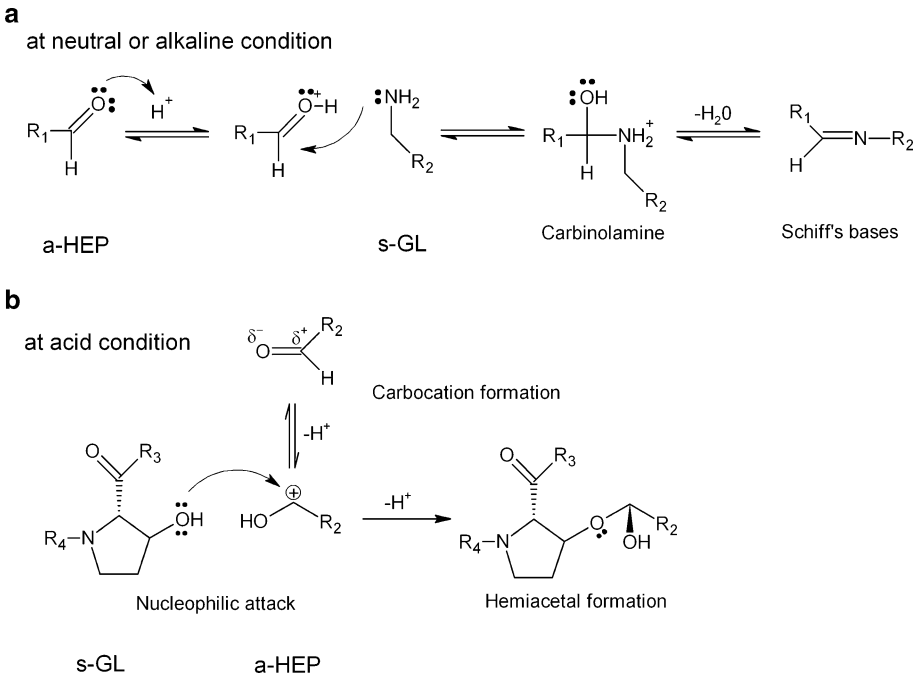

Fig. 3 Reaction mechanism **a** between amino groups of succinyl gelatin and aldehyde groups of a-HEP for the formation of Schiff base at pH 5.0, 7.4 and 10.0 and **b** between hydroxyl groups of s-GL and aldehyde groups of a-HEP at pH 2.5

stabilization of the NPs. At this acidic status, most of the amino groups are protonated and cannot react with aldehyde groups. But we assume that there are still some free amino groups involved in Schiff base reaction to form cross-linked NPs at equilibrium conditions.

Cross-linked s-GL/a-HEP NPs were prepared in water/acetone by simply adjusting pH values during the reaction. Parameters such as surfactant (Pluronics) concentration (0, 0.1 and 1 % w/v), s-GL concentration (0.5 and 5 % w/v), volume ratio of acetone/water (1:1, 2:1 and 3:1) and molar ratio of a-HEP/s-GL (10:2.3, 5:2.3 and 1:2.3) were varied to optimize the condition of NPs formation, which also influenced the stability of s-GL/a-HEP NPs suspensions. The results showed that a high concentration of s-GL (5 % w/v) without any surfactant lead to aggregation in water/acetone at either pH 2.5 or 7.4 before addition of the a-HEP as a cross-linker. Therefore, a lower concentration of s-GL of 0.5 % w/v was chosen and combined with two concentrations of surfactant (Pluronics F68), such as 0.1 and 1 % w/v. Pluronics F68 is a non-ionic surfactant, which contains a central hydrophobic block of polypropylene oxide (PPO) and two identical hydrophilic blocks of polyethylene oxide (PEO) at both sides. Without F68, the solution was unstable after the addition of the cross-linker (a-HEP), while after adding the surfactant, stable solutions were obtained. At low concentration of 0.1 % w/v, F68 contributed to stabilization of the s-GL emulsions at different pH value probably via the hydrophobic interaction between the PPO fragment and hydrophobic residues of s-GL [40], resulting in NPs of a size around 200 nm determined by DSL (Table 2). However, at high F 68 concentration of 1.0 % w/v, the particle size increased from 196.3 nm to 372.2 nm at pH 2.5 and from 202.4 nm to large aggregates at pH 7.4, respectively. The size distribution also increased significantly from 0.123 to 0.232 nm at pH 2.5 and from 0.257 to 0.646 nm at pH 7.4. The larger diameter and broader size distributions of NPs indicated that an excess of surfactant increased the diameter of cross-linked NPs. This was not beneficial to form NPs of a homogeneous size.

Table 2 Effects of pH conditions and Pluronics F68 concentrations on the Z-average diameter and polydispersity index (PDI) of s-GL/a-HEP NPs

pH	0.1 % (w/v) Pluronics F68		1 % (w/v) Pluronics F68	
	Z-average[a] (d. nm)	PDI[a]	Z-average[a] (d. nm)	PDI[a]
2.50	196.3	0.123	372.2	0.232
5.00	283.7	0.301	–	–
7.40	202.4	0.257	–	0.646
10.00	210.6	0.351	–	–

[a] Size (Z-average) and size distribution (PDI) determined by the DLS method

Aggregation of particles was also observed in the solution when the molar ratio of –CHO/–NH_2 was increased from 1:2.3 to 10:2.3 due to excess amount of cross-linker of a-HEP. In the end, 0.1 % w/v Pluronics F68, 0.5 % w/v s-GL, 2:1 v/v acetone/water and 1:2.3 of –CHO/–NH_2 (a-HEP/s-GL) were chosen for particle synthesis. Under this condition, four different pH values applied during particle

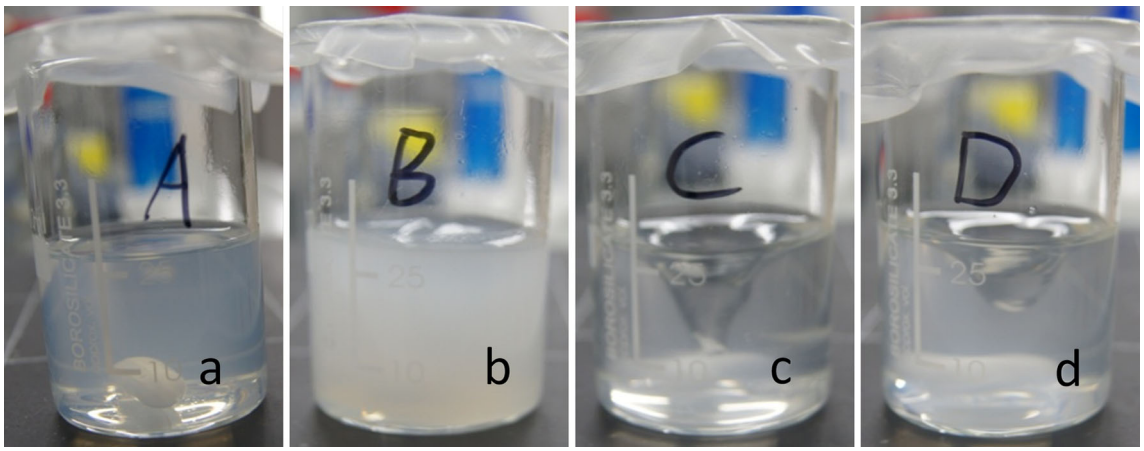

Fig. 4 Photos of s-GL solution containing 0.1 % (w/v) Pluronics F68 were cross-linked by a-HEP at **a** pH 2.5, **b** pH 5.0, **c** pH 7.4 and **d** pH 10.0

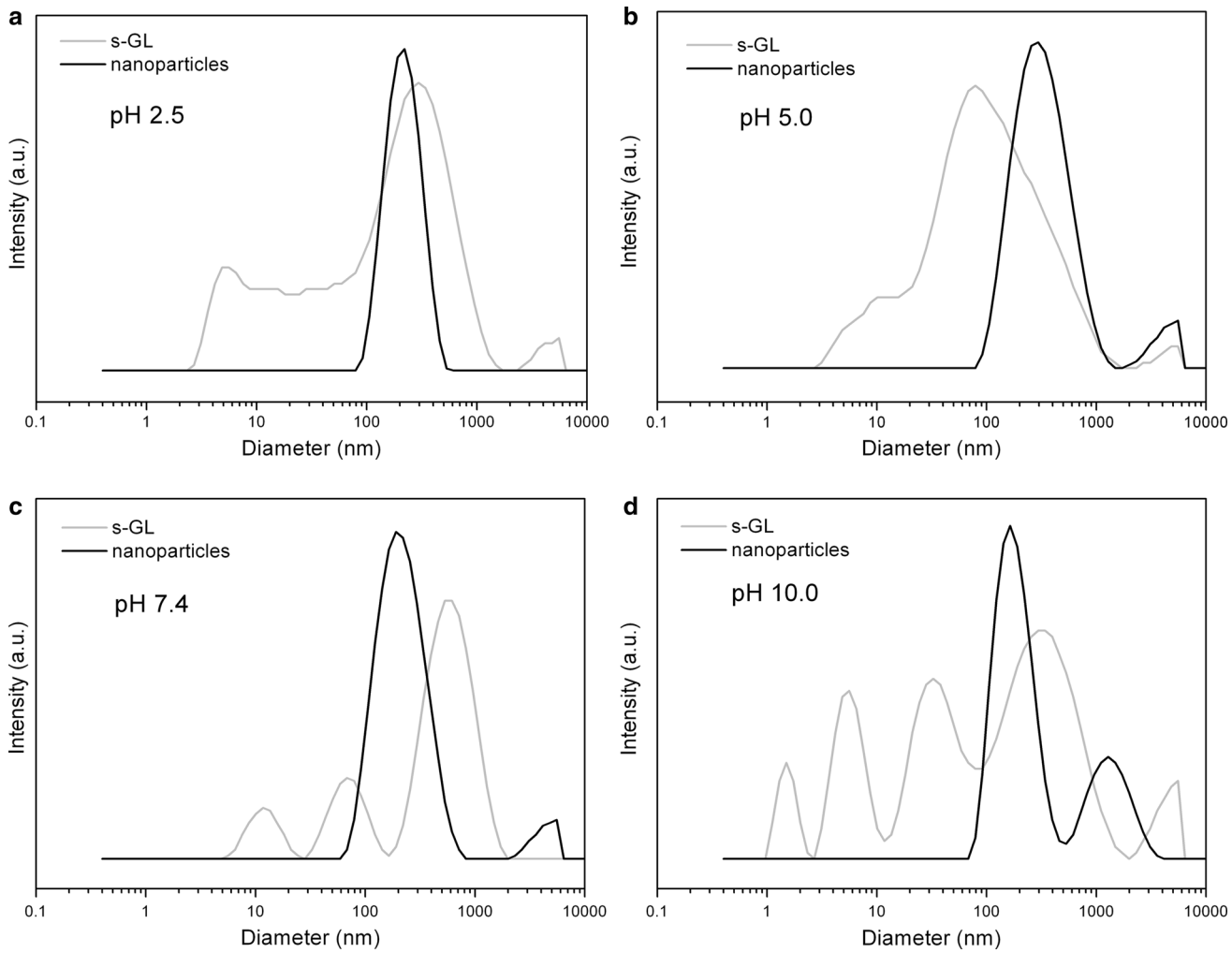

Fig. 5 DLS measurements of s-GL solution of concentration 1 mg/mL (*gray line*) and s-GL/a-HEP NPs of concentration 1–5 mg/mL (*black line*) at different pH values, **a** pH 2.5, **b** pH 5.0, **c** pH 7.4, **d** pH 10.0

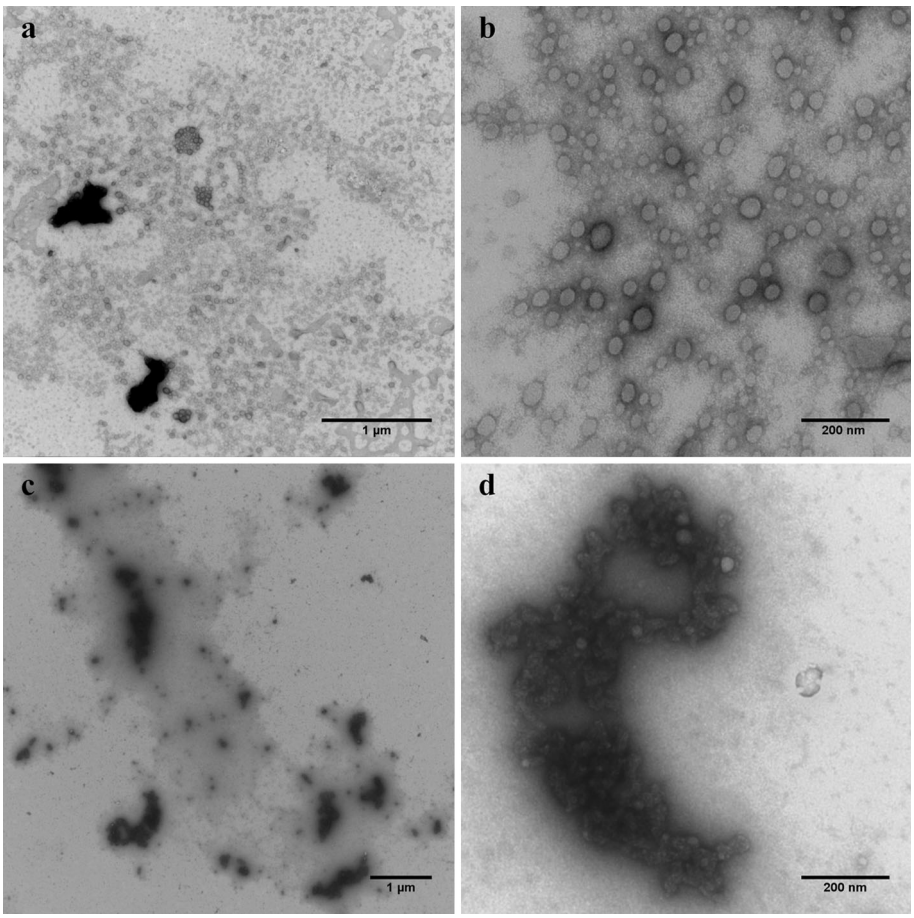

Fig. 6 TEM images of s-GL/a-HEP NPs prepared at different pH conditions **a**, **b** NPs well distributed at pH 2.5 and **c**, **d** NPs formed large aggregation at pH 7.4: **a**, **c** images over large regions of scale bar 1 μm and **b**, **d** images of characteristic regions of scale bar 200 nm, respectively

formation were compared. The macroscopic appearance of these solutions is shown in Fig. 4. At pH 5.0, aggregation in the solution was observed after addition of acetone. The isoelectric point (IEP) of s-GL is around 4.0 (see Fig. S1) and near this pH, s-GL has the minimum solubility. Far away from IEP of gelatin, stable emulsions were formed at pH 2.5, 7.4 and 10.0, respectively.

Figure 5 and Table 2 show the size distribution of s-GL and cross-linked s-GL/a-HEP NPs under various pH conditions. We can see that every peak of s-GL before cross-linking (PDI are nearly 1), whether single or multiple, are broad (grey lines in Fig. 5a–d). Gelatin is a hydrolysis product of collagen with large variance in molecular weight, thus it is a challenge to fabricate uniform NPs. Coester et al. [30] developed a two-step desolvation method and successfully formed uniform and stable NPs. In our study, we chemically modified the gelatin and then used dialysis to separate the gelatin of large molecular weight from small molecular weight ones. The gelatin no less than 177 kDa was kept for forming NPs. After cross-linking, s-GL/a-HEP NPs have narrow size distributions at all pH conditions (black lines in Fig. 5a–d).The diameters of s-GL/a-HEP NPs were in the range of 200–300 nm (see Table 2), depending on pH values. The net charge of s-GL in solution is strongly affected by the prevalent pH conditions, which led to the alterations in final particle size. At pH 2.5, the NPs have uniform particle size and a well dispersed character (Fig. 5a) (Z-average 196.3 nm, PDI 0.123), which is smallest among all. At pH 5.0, the produced NPs strongly tended to aggregation and precipitation, which ended up with an average size of 283.7 nm. The PDI is 0.301 (Fig. 5b), indicating high heterogeneity. s-GL is neutral at around pH 4.0. Under this condition, the remaining net charge of s-GL was too weak to prevent the freshly formed cross-linked NPs from large aggregation. Above pH 5.0, for example 7.4 and 10.0, cross-linked NPs slightly increased in size compared to those at pH 2.5, while the size distribution was broaden with pH increasing (Fig. 5c, d). The amino groups on NPs' surface are neutral and easily react with a-HEP, which might cause them

cross-linked to each other and form large aggregation, which were also observed from TEM, as shown in Fig. 6c, d.

The TEM images of s-GL/a-HEP cross-linked NPs in Fig. 6 further demonstrate that the change of pH value can lead to different morphology of NPs. At pH 2.5, the NPs showed a spherical shape of an average particle size ~50 nm (Fig. 6 a, b); while at pH 7.4, they showed large aggregation of size around 1 μm consisting of a number of smaller particles of sizes approximately 30–40 nm (Fig. 6 c, d). In general, during TEM the particles were shrinking largely (size approximately 50 nm) compared with the size in solution (approximately 200 nm, measured by DLS) at pH 2.5 and 7.4. The shrinking of NPs under dry condition was also observed by Coester et al. [30] when they used scanning electron microscopy to examine gelatin NPs.

The free amino group content of s-GL/a-HEP NPs prepared at different pH conditions was determined by TNBS test. The degree of cross-linking of NPs was then calculated from Eq. (1) and is listed in Table 3. The experimental degrees of cross-linking, 13.3 % and 19.4 %, were lower than the expected, 43.5 %. The degree of cross-linking at pH 2.5 (13.3 %) was lower than that at pH 7.4 (19.4 %), which may be due to the different cross-linking mechanisms [39]. At pH 2.5, most of amino groups are protonated ($-NH_3^+$) so that they cannot react with aldehyde groups and thus the NPs displayed a positive zeta potential 7.3 ± 3.0 mV (Table 3). Those $-NH_3^+$ groups were then deprotonated and tested by TNBS assay at pH 9. In additional, at acid condition, most of hydroxyl groups instead of amino groups were cross-linked with aldehyde groups and there quantity cannot be easily measured. On the other hand, at neutral or alkaline condition, primary amino groups reacted with aldehyde groups and raised the degree of cross-linking over the one at lower pH, according to TNBS test. After cross-linking, the remaining amino groups of s-GL were in neutral status, while the carboxyl groups (from s-GL and a-HEP) and sulfate groups (from a-HEP) were deprotonated. Therefore, the NPs showed a negative zeta potential of −2.6 ± 0.3 mV at pH 7.4. Due to different mechanisms, the real cross-linking degree cannot be detected easily, especially at acidic condition.

Table 3 Theoretical (D_{th}) and experimental (D_{exp}) degree of cross-linking and zeta potentials of s-GL/a-HEP NPs at different pH conditions

pH	Free $-NH_2$ groups of s-GL ($\times 10^{-4}$ mol/g)	Free $-NH_2$ groups of s-GL/a-HEP NPs ($\times 10^{-4}$ mol/g)[a]	D_{th} (%)	D_{exp} (%)	Zeta-potential (mV)[b]
2.5	1.08	0.936	43.5	13.3	7.3 ± 3.0
7.4	1.08	0.870	43.5	19.4	−2.6 ± 0.3

[a] The remaining amino groups content of s-GL/a-Hep NPs was determined via using TNBS assay by UV–Vis spectroscopy at 365 nm. L-lysine was used as the standard substance

[b] Zeta-potential measured by a zetasizer with three trials

3.3 Hydroxyapatite mineralization on cross-linked NPs

The particles synthesized at pH 2.5 were used for further mineralization. The whole process is shown in Fig. 7. (a) s-GL/a-HEP NPs formed at pH 2.5 with a positive zeta potential due to the protonation of amino groups and carboxylic acid groups within s-GL. (b) When pH increased to 10.0 with $NH_3 \cdot H_2O$, $-NH_3^+$ became $-NH_2$ and –COOH or $-SO_3H$ were deprotonated. Therefore, NPs displayed a negative charge. (c) $Ca(NO_3)_2$ was added and the negatively charged particles attracted Ca^{2+} due to Coulomb attraction [2]. (d) $(NH_4)_2HPO_4$ was added and PO_4^{3-} interacted with Ca^{2+} to start mineralization. Finally, HAP was formed on the cross-linked NPs [2, 8].

At different time points of reaction (0.5, 1, 4 and 24 h), a certain amount of sample solution was recovered, kept in −80 °C freezer for 2 days and subsequently freeze-dried overnight. The mineralized products were analyzed by FTIR and XRD and the results are shown in Figs. 8 and 9. For s-GL/a-HEP NPs (Fig. 8a), the adsorption bands at 1,657; 1,542; and 1,239 cm^{-1} were associated to amide I [ν(C=O)], amide II [δ(NH) and ν(N–C=O)] bands of s-GL, respectively. The typical peaks at 1,235 cm^{-1} [overlay with ν(N–C=O)] and 1,032 cm^{-1} related to symmetric and

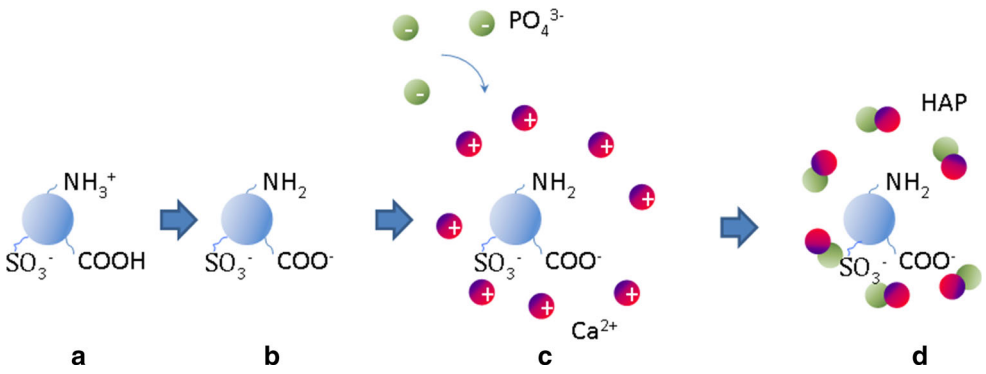

Fig. 7 Schematic picture of bio-mineralization process on s-GL/a-HEP NPs

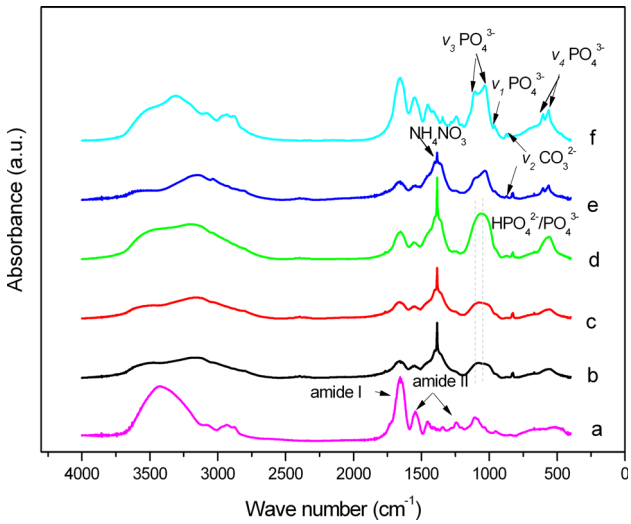

Fig. 8 FTIR spectrums of (*a*) s-GL/a-HEP NPs, and HAP mineralization on s-GL/a-HEP NPs at different time intervals (*b*) at 0.5 h, (*c*) at 1 h, (*d*) at 4 h, (*e*) at 24 h before dialysis (*f*) at 24 h and subsequently dialysis for 24 h

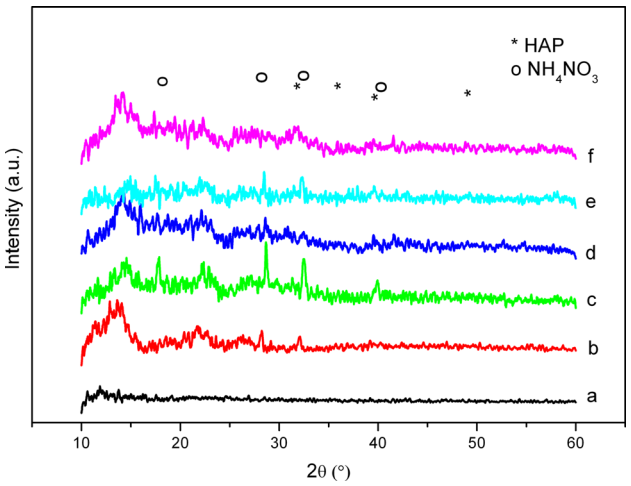

Fig. 9 X-ray diffraction spectrum of (*a*) s-GL NPs, and HAP mineralization on s-GL/a-HEP NPs at different time intervals (*b*) at 0.5 h, (*c*) at 1 h, (*d*) at 4 h, (*e*) at 24 h before dialysis, and (*f*) at 24 h and subsequently dialysis for 24 h

asymmetric stretching absorptions of sulfate groups within a-HEP. Therefore, intermolecular and/or intramolecular bridges between s-GL are formed through the cross-linking by a-HEP and result in the stable shell of NPs.

Comparing to the FTIR spectra of s-GL/a-HEP NPs (Fig. 8a), after mineralization for different periods of time, a broad band appeared in the region of 1,115 to 1,030 cm^{-1} after 0.5–4 h, which might be related to HPO_4^{2-}/PO_4^{3-} mixed phase [31], indicating the formation of a precursor of HAP. After 24 h mineralization (Fig. 8 e, f), this broad band split into two distinguished peaks at 1,093 and 1,033 cm^{-1}, respectively, which were associated to v_3 asymmetric stretching of PO_4^{3-} ions, suggesting the transformation of HPO_4^{2-}–PO_4^{3-} (Fig. 8f). In addition we also observed the weak band of v_1 symmetric stretching PO_4^{3-} at 970 cm^{-1}, degenerated v_4 bending PO_4^{3-} at 604 and 563 cm^{-1}, respectively, suggesting the presence of a apatite-like phase [6, 41, 42]. Figure 8e shows that NH_4NO_3 was formed and showed a peak at 1,384 cm^{-1} due to N–O covalent bond, but after dialysis it was removed from the particles (Fig. 8f) [43]. During the co-precipitation process of HAP on s-GL/a-HEP NPs, the Ca^{2+} ions can interact with $–COO^-$ of s-GL and a-HEP, as well as $-SO_3^{2-}$ of a-HEP. The doubly degenerated v_2 CO_3^{2-} bending mode at 877 cm^{-1} (Fig. 8 e–f) indicated the formation of a B-type carbonate HAP on the NPs [41, 44], which is the main biological apatite found in the bone or tooth [45]. Unlike gelatin or collagen inducing HAP that only provide $R\text{-}COO^-$ nucleation site, we assume that the additional $-SO_3^{2-}$ groups of a-HEP can provide a new nucleation site for the growth of HAP crystals. There is a very weak band at 672 cm^{-1}, which might be associated to calcium sulfate complex [46]. But its typical bands at around 1,010 cm^{-1} were overlaid by the bands of PO_4^{3-} [46]. Therefore, to confirm such complex, the samples should be further subjected to Raman spectroscopy. Moreover, the cross-linking induces to shorten the distances between s-GL/a-HEP network and so more amount of Ca^{2+} have a chance to bind to protein/GAG matrix, which might be favor to form the well-ordered HAP crystals.

There is no characteristic sharp peak found in the spectra of organic s-GL/a-HEP NPs, which is typical for amorphous polymer lacking of crystalline phase (Fig. 9a). Figure 9b–f shows that the peaks at 25.9°(002), 32.1°(211), 40.0°(310) and 50°(004) were associated to HAP according to XRD database JCP 2.2 CA, indicating that HAP formation on NPs over time. s-GL/a-HEP NPs acting as individual nano-template are suitable for HAP crystallization. The NPs are loaded with calcium ions by complexation with the carboxyl or sulfate groups present either in s-GL or in a-HEP chains. Further addition of phosphate ions leaded to the formation of calcium phosphate.

The solution composed of $Ca(NO_3)_2{\cdot}4H_2O$ and $(NH_4)_2HPO_4$ can be mediated to transform HAP, which is thermodynamically stable. The time dependent crystallite growth can also be determined with the sharpness of the peaks in Fig 9 b–e. NH_4NO_3 as a side product also have peaks at 17.7°, 22.3°, 28.6° and 39.3° based on XRD database. However, after dialysis, all its characteristic peaks disappeared. The HAP peaks show that its intensity is very low, which may be the result of little HAP in the sample. But it is important to note that the local Ca^{2+} concentration around the NPs surfaces is higher than that in the surrounding solution, which can be in favor of its

bounding to functional groups of NPs, and thus nucleation takes place. Combining the results from FTIR and XRD, we demonstrate that HAP has been formed.

4 Conclusions

In this study NPs were formed by cross-linking s-GL with oxidized heparin via Schiff's base linkage. The obvious advantage of this method is that small toxic cross-linkers like glutardialdehyde are not needed while the aldehyde groups of the larger oxidized GAG do not express a toxicity in vitro as shown in previous investigations [24].The process of nanoparticle formation could be optimized here regarding particle size and colloidal stability selecting a pH of 2.5, 0.5 % w/v s-GL and a ratio of 1:2.3 n(–CHO)/n(–NH_2) to obtain a mean particle size of 198 nm. These NPs were further used as nano-reactor for promoting the growth of HAP crystals. The mineralization process was done in a solution composed of $Ca(NO_3)_2$ and $(NH_4)_2HPO_4$. The NPs provided probably nucleation sites through their carboxyl and sulfate groups to form thermally-stable B-type HAP on them without calcination. Future studies with these NPs will be conducted to test their applicability for controlled release of growth factors with heparin-binding domains like BMP-2 or FGF-2 and their intermixing with hydrogels, which can be injected into bone defects.

Acknowledgments We are very thankful to Dr. Hendrik Metz for zeta potential experiment, Mrs. Ute Mentzel for FFFF and DLS measurements and Ms. Kristin Wendt for XRD analysis. This work was supported by the European Union Seventh Framework Program (FP7/2007–2013) under Grant agreement no. NMP4-SL-2009-229292 ("Find and Bind").

References

1. Ryu J, Kim SW, Kang K, Park CB. Mineralization of self-assembled peptide nanofibers for rechargeable lithium ion batteries. Adv Mater. 2010;22(48):5537–41. doi:10.1002/adma.201000669.
2. Scholler K, Ethirajan A, Zeller A, Landfester K. Biomimetic route to calcium phosphate coated polymeric nanoparticles: influence of different functional groups and pH. Macromol Chem Phys. 2011;212(11):1165–75. doi:10.1002/macp.201100109.
3. Zietz C, Bergschmidt P, Lange R, Mittelmeier W, Bader R. Third-body abrasive wear of tibial polyethylene inserts combined with metallic and ceramic femoral components in a knee simulator study. Int J Artif Organs. 2013;36(1):47–55. doi:10.5301/ijao.5000189.
4. Liu H, Li H, Cheng WJ, Yang Y, Zhu MY, Zhou CR. Novel injectable calcium phosphate/chitosan composites for bone substitute materials. Acta Biomater. 2006;2(5):557–65.
5. Legeros RZ, Lin S, Rohanizadeh R, Mijares D, Legeros JP. Biphasic calcium phosphate bioceramics: preparation, properties and applications. J Mater Sci. 2003;14(3):201–9.
6. Li WM, Chen SY, Liu DM. In situ doxorubicin-CaP shell formation on amphiphilic gelatin-iron oxide core as a multifunctional drug delivery system with improved cytocompatibility, pH-responsive drug release and MR imaging. Acta Biomater. 2013;9(2):5360–8. doi:S1742-7061(12)00460-6.
7. Azami M, Samadikuchaksaraei A, Poursamar SA. Synthesis and characterization of a laminated hydroxyapatite/gelatin nanocomposite scaffold with controlled pore structure for bone tissue engineering. Int J Artif Organs. 2010;33(2):86–95.
8. Boanini E, Bigi A. Biomimetic gelatin–octacalcium phosphate core-shell microspheres. J Colloid Interface Sci. 2011;362(2):594–9.
9. Ethirajan A, Ziener U, Chuvilin A, Kaiser U, Colfen H, Landfester K. Biomimetic hydroxyapatite crystallization in gelatin nanoparticles synthesized using a miniemulsion process. Adv Funct Mater. 2008;18(15):2221–7.
10. Nitta SK, Numata K. Biopolymer-based nanoparticles for drug/gene delivery and tissue engineering. Int J Mol Sci. 2013;14(1):1629–54.
11. Kadengodlu PA, Aigaki T, Abe H, Ito Y. Cationic cholesterol-modified gelatin as an in vitro siRNA delivery vehicle. Mol Biosyst. 2013;9(5):965–8. doi:10.1039/c2mb25424g.
12. Tan GK, Tabata Y. Effect of gelatin microsphere size and cell/microsphere ratio on transforming growth factor-beta-3-induced chondrogenesis of human mesenchymal stem cells. J Tissue Eng Regen Med. 2012;6:67.
13. Solorio LD, Vieregge EL, Dhami CD, Dang PN, Alsberg E. Engineered cartilage via self-assembled hMSC sheets with incorporated biodegradable gelatin microspheres releasing transforming growth factor-beta 1. J Controlled Release. 2012;158(2):224–32.
14. Lee ES, Gao ZG, Bae YH. Recent progress in tumor pH targeting nanotechnology. J Controlled Release. 2008;132(3):164–70.
15. Kawadkar J, Jain R, Kishore R, Pathak A, Chauhan MK. Formulation and evaluation of flurbiprofen-loaded genipin cross-linked gelatin microspheres for intra-articular delivery. J Drug Target. 2013;21(2):200–10. doi:10.3109/1061186X.2012.745549.
16. Guillame-Gentil O, Semenov O, Roca AS, Groth T, Zahn R, Voros J, et al. Engineering the extracellular environment: strategies for building 2D and 3D cellular structures. Adv Mater. 2010;22(48):5443–62. doi:10.1002/adma.201001747.
17. Hudalla GA, Murphy WL. Biomaterials that Regulate Growth Factor Activity via Bioinspired Interactions. Adv Funct Mater. 2011;21(10):1754–68.
18. Lever R, Page CR. Novel drug development opportunities for heparin. Nat Rev Drug Discov. 2002;1(2):140–8.
19. Raman K, Mencio C, Desai UR, Kuberan B. Sulfation patterns determine cellular internalization of heparin-like polysaccharides. Mol Pharm. 2013;. doi:10.1021/mp300679a.
20. Kanzaki S, Ariyoshi W, Takahashi T, Okinaga T, Kaneuji T, Mitsugi S, et al. Dual effects of heparin on BMP-2-induced osteogenic activity in MC3T3-E1 cells. Pharmacol Rep. 2011;63(5):1222–30.
21. Jeon O, Song SJ, Yang HS, Bhang SH, Kang SW, Sung MA, et al. Long-term delivery enhances in vivo osteogenic efficacy of bone morphogenetic protein-2 compared to short-term delivery. Biochem Biophys Res Commun. 2008;369(2):774–80.
22. Liu ZM, Gu QY, Xu ZK, Groth T. Synergistic effect of polyelectrolyte multilayers and osteogenic growth medium on differentiation of human mesenchymal stem cells. Macromol Biosci. 2010;10(9):1043–54.
23. Kisiel M, Martino MM, Ventura M, Hubbell JA, Hilborn J, Ossipov DA. Improving the osteogenic potential of BMP-2 with hyaluronic acid hydrogel modified with integrin-specific fibronectin fragment. Biomaterials. 2013;34(3):704–12.
24. Kowitsch A, Yang Y, Ma N, Kuntsche J, Mader K, Groth T. Bioactivity of immobilized hyaluronic acid derivatives regarding protein adsorption and cell adhesion. Biotechnol Appl Biochem. 2011;58(5):376–89.

25. Xiao JW, Zhu YC, Ruan QC, Liu YY, Zeng Y, Xu FF, et al. Biomacromolecule and surfactant complex matrix for oriented stack of 2-dimensional carbonated hydroxyapatite nanosheets as alignment in calcified tissues. Cryst Growth Des. 2010;10(4):1492–9.
26. Jia XQ, Burdick JA, Kobler J, Clifton RJ, Rosowski JJ, Zeitels SM, et al. Synthesis and characterization of in situ cross-linkable hyaluronic acid-based hydrogels with potential application for vocal fold regeneration. Macromolecules. 2004;37(9):3239–48.
27. Sashidhar RB, Capoor AK, Ramana D. Quantitation of epsilon-amino group using amino-acids as reference-standards by trinitrobenzene sulfonic-acid—a simple spectrophotometric method for the estimation of hapten to carrier protein ratio. J Immunol Methods. 1994;167(1–2):121–7.
28. Croy SR, Kwon GS. The effects of Pluronic block copolymers on the aggregation state of nystatin. J Control Release. 2004;95(2):161–71.
29. Ethirajan A, Schoeller K, Musyanovych A, Ziener U, Landfester K. Synthesis and optimization of gelatin nanoparticles using the miniemulsion process. Biomacromolecules. 2008;9(9):2383–9.
30. Coester CJ, Langer K, van Briesen H, Kreuter J. Gelatin nanoparticles by two step desolvation—a new preparation method, surface modifications and cell uptake. J Microencapsul. 2000;17(2):187–93. doi:10.1080/026520400288427.
31. Kim DW, Cho IS, Kim JY, Jang HL, Han GS, Ryu HS, et al. Simple large-scale synthesis of hydroxyapatite nanoparticles. In situ observation of crystallization process. Langmuir. 2010;26(1):384–8.
32. Habeeb AFS. Determination of free amino groups in proteins by trinitrobenzenesulfonic acid. Anal Biochem. 1966;14(3):328. doi:10.1016/0003-2697(66)90275-2.
33. Lu SY, Liu MZ, Ni BL. An injectable oxidized carboxymethylcellulose/*N*-succinyl-chitosan hydrogel system for protein delivery. Chem Eng J. 2010;160(2):779–87.
34. Sui WP, Wang YH, Dong S, Chen YJ. Preparation and properties of an amphiphilic derivative of succinyl-chitosan. Colloids Surf A. 2008;316(1–3):171–5.
35. Harada NS, Oyama HT, Bartoli JR, Gouvea D, Cestari IA, Wang SH. Quantifying adsorption of heparin on a PVC substrate using ATR-FTIR. Polym Int. 2005;54(1):209–14.
36. Wang DA, Varghese S, Sharma B, Strehin I, Fermanian S, Gorham J, et al. Multifunctional chondroitin sulphate for cartilage tissue-biomaterial integration. Nat Mater. 2007;6(5):385–92.
37. Kale R, Bajaj A. Ultraviolet spectrophotometric method for determination of gelatin crosslinking in the presence of amino groups. J Young Pharm. 2010;2(1):90–4. doi:10.4103/0975-1483.62223.
38. Bubnis WA, Ofner CM. The determination of epsilon-amino groups in soluble and poorly soluble proteinaceous materials by a spectrophotometric method using trinitrobenzenesulfonic acid. Anal Biochem. 1992;207(1):129–33.
39. Farris S, Song J, Huang Q. Alternative reaction mechanism for the cross-linking of gelatin with glutaraldehyde. J Agric Food Chem. 2010;58(2):998–1003. doi:10.1021/jf9031603.
40. Griffiths PC, Fallis IA, Teerapornchaisit P, Grillo I. Hydrophobically modified gelatin and its interaction in aqueous solution with sodium dodecyl sulfate. Langmuir. 2001;17(9):2594–601.
41. Dasgupta S, Banerjee SS, Bandyopadhyay A, Bose S. Zn- and Mg-doped hydroxyapatite nanoparticles for controlled release of protein. Langmuir. 2010;26(7):4958–64. doi:10.1021/la903617e.
42. Rehman I, Bonfield W. Characterization of hydroxyapatite and carbonated apatite by photo acoustic FTIR spectroscopy. J Mater Sci. 1997;8(1):1–4.
43. Wu HB, Chan MN, Chan CK. FTIR characterization of polymorphic transformation of ammonium nitrate. Aerosol Sci Technol. 2007;. doi:10.1080/02786820701272038.
44. Chang MC, Tanaka J. FT-IR study for hydroxyapatite/collagen nanocomposite cross-linked by glutaraldehyde. Biomaterials. 2002;23(24):4811–8.
45. LeGeros RZ. Calcium phosphates in oral biology and medicine. Monogr Oral Sci. 1991;15:1–201.
46. Rodriguez A, Eremin K, Khandekar N, Stenger J, Newman R, Bazeta F, et al. Characterization of calcium sulfate grounds and fillings of applied tin-relief brocades by Raman spectroscopy, Fourier transform infrared spectroscopy, and scanning electron microscopy. J Raman Spectrosc. 2010;41(11):1517–24.